Journal of Materials Chemistry A

Accepted Manuscript

ROYAL SOCIETY OF CHEMISTRY

www.rsc.org/materialsA

Kinetic Analysis of Photoelectrochemical Water Oxidation by Mesostructured Co-Pi/α-Fe_2O_3 Photoanodes

Gerard M. Carroll and Daniel R. Gamelin*

Department of Chemistry, University of Washington, Seattle, WA 98195-1700

Email: gamelin@chem.washington.edu

Abstract. Solar water splitting using catalyst-modified semiconductor photoelectrodes is a promising approach to harvesting and storing solar energy. Prior studies have demonstrated that modification of α-Fe_2O_3 photoanodes with the water-oxidation electrocatalyst Co-Pi enhances photon-to-current conversion efficiencies, particularly at less positive potentials, but the mechanism underlying this enhancement remains poorly understood. Different experimental techniques have suggested very different interpretations of the microscopic origins of this improvement. Here, we report results from photoelectrochemical and impedance measurements aimed at understanding the Co-Pi/α-Fe_2O_3 interface of mesostructured composite photoanodes. Contrary to expectations, these measurements reveal that α-Fe_2O_3 water-oxidation kinetics actually slow upon deposition of Co-Pi, but electron-hole recombination slows even more, resulting in a net enhancement of water-oxidation quantum efficiency. The negative shift in the *J-V* curve caused by Co-Pi deposition is found to result from the introduction of an alternative pathway for water oxidation catalyzed by Co-Pi, which allows the composite photoanode to avoid positive charge accumulation at the α-Fe_2O_3 surface. We detail the role of Co-Pi thickness optimization in balancing the slower recombination against the slower water oxidation kinetics to achieve the lowest water-oxidation onset potential. These results provide new insights into the microscopic properties of the catalyst/semiconductor interface in Co-Pi/α-Fe_2O_3 composite solar water-splitting photoanodes.

Introduction

Photoelectrochemical (PEC) water splitting has been proposed as a promising strategy for harvesting and storing solar energy.[1-6] Hematite (α-Fe_2O_3) has emerged as a model system for the water-oxidation half reaction in PEC water-splitting cells. With a band gap of 2.1 eV, stability under operating conditions, and a valence-band potential ~1.6 V more positive than the thermodynamic water-oxidation potential (+1.23 V), α-Fe_2O_3 balances many of the necessary criteria for PEC applications.[7-11] Owing to its poor electron mobility (10^{-2} to 10^{-1} $cm^2s^{-1}V^{-1}$),[12] short hole-diffusion lengths (2-20 nm),[13,14] and slow water-oxidation kinetics, however,[15-22] the solar-to-hydrogen efficiencies of α-Fe_2O_3 PEC cells are typically low, suffering greatly from electron-hole recombination within the bulk and at the semiconductor/liquid junction (SCLJ).

Recently, the strategy of interfacing α-Fe_2O_3 and related photoanodes with water-oxidation catalysts to improve their PEC performance has attracted tremendous attention.[23-26] Interfacing mesostructured α-Fe_2O_3 with the earth-abundant, self-healing, and ion-permeable amorphous water-oxidation electrocatalyst cobalt phosphate (Co-Pi)[27-30] shifts the water-oxidation onset potential in the negative direction by ~100-150 mV.[7,31,32] Optimization of the Co-Pi thickness is necessary because PEC water-oxidation onset potentials can actually increase when the Co-Pi layer is too thick, depending on the active surface area of the α-Fe_2O_3 photoelectrode.[33]

Despite advances in the development of Co-Pi/α-Fe_2O_3 and related composite photoanodes showing improved water-oxidation current densities at more negative potentials, it remains unclear *how* Co-Pi enhances water-oxidation rates at low potentials. Initial reports hypothesized that Co-Pi catalyzes water oxidation at the α-Fe_2O_3 surface.[7,31,32] An alternative hypothesis suggests that Co-Pi is instead a spectator in the water-oxidation catalysis, and its primary role is to increase α-Fe_2O_3 band bending near the SCLJ, resulting in reduced surface electron-hole recombination and a negatively shifted water-oxidation onset potential.[20,21,34,35] This hypothesis stems from transient absorption measurements on mesostructured α-Fe_2O_3 photoanodes showing that Co-Pi prolongs the lifetimes of photogenerated holes to timescales (0.1 - 1.0 s) that resemble those of the bare α-Fe_2O_3 photoanodes under positive bias.[20,21,34,36] Charge transfer from α-Fe_2O_3 to Co-Pi is not invoked in this hypothesis. Similar conclusions were drawn in an independent study employing intensity-modulated photocurrent spectroscopy.[37] α-Fe_2O_3 surface passivation with non-catalytic layers does shift the PEC water-oxidation onset potential more negative,[15] confirming this general mechanism for α-Fe_2O_3,[38] but impedance and transient photocurrent

spectroscopies have also demonstrated capacitive charging of the Co-Pi layer in planar Co-Pi/α-Fe_2O_3 photoanodes, confirming hole transfer to Co-Pi.[39] Similarly, dual-potentiostat measurements have shown that Co-Pi forms an 'adaptive junction' with hematite, which relies on ion permeability and capacitive hole storage in Co-Pi.[24,40] Measurements of the PEC water-oxidation pH dependence further show a change in the microscopic mechanism with Co-Pi deposition, confirming water oxidation directly by Co-Pi in mesostructured Co-Pi/α-Fe_2O_3 photoanodes.[33] Lastly, the current-potential behavior with increasing Co-Pi thickness has been shown to depend strongly on the surface morphology of the underlying photoanode.[33] This observation undermines assumptions that planar and highly structured Co-Pi/α-Fe_2O_3 photoanodes behave in the same way.[18,35,38] Additional characterization of mesostructured Co-Pi/α-Fe_2O_3 photoanodes is therefore warranted. The role of Co-Pi thus appears more rich and complex than originally anticipated, and to date, no single model can account for all of the experimental observations made on Co-Pi/α-Fe_2O_3 composite water-oxidation photoanodes.

Here, we report the results of photoelectrochemical (PEC) and photoelectrochemical impedance spectroscopy (PEIS) measurements on mesostructured Co-Pi/α-Fe_2O_3 photoanodes aimed at understanding the impact of Co-Pi at this interface. The data suggest that the negative shift in onset potential with Co-Pi deposition is related to facile charge transfer to Co-Pi followed by Co-Pi-catalyzed water oxidation. At low potentials, the trap-state-mediated charge-transfer mechanism for water oxidation at the surface of α-Fe_2O_3 is bypassed upon Co-Pi addition, resulting in both an increase in band bending *and* a decrease in trap-centered surface recombination, confirming aspects of both hypotheses presented above. Contrary to expectations, the data show that the PEC water-oxidation kinetics actually *slow* upon addition of Co-Pi to the α-Fe_2O_3 surface, but the surface electron-hole recombination slows even more, such that the quantum efficiency for PEC water oxidation at low potentials increases. Finally, these measurements show that thick layers of Co-Pi inhibit catalytic turnover by allowing increased interfacial recombination between Co-Pi holes and α-Fe_2O_3 conduction-band electrons, a behavior greatly exacerbated by the high surface areas of these mesostructured photoanodes. These results help tie together many of the disparate observations made in previous studies of Co-Pi/α-Fe_2O_3 composite water-oxidation photoanodes, improving the fundamental understanding of this complex interface.

Experimental

Synthesis. Mesostructured silicon-doped α-Fe_2O_3 photoanodes were fabricated on fluorine-doped tin oxide (FTO) coated glass (TEC 15, Hartford Glass Co.) by an atmospheric pressure chemical vapor deposition (APCVD) method described previously.[7,31,41] The APCVD synthesis was modified to yield α-Fe_2O_3 photoanodes optimized for backside illumination (through the FTO). This optimization was achieved by decreasing the deposition period to ~70% of the typical deposition time, thus producing thinner α-Fe_2O_3 films. To prepare the Co-Pi/α-Fe_2O_3 composite photoanodes, Co-Pi was deposited onto α-Fe_2O_3 photoanodes by photo-assisted electrodeposition under calibrated 1-sun simulated AM1.5 solar irradiation through the back side of the sample. All Co-Pi depositions were carried out at a constant current of 6 μA/cm^2 from a solution of 0.5 mM cobalt nitrate in 0.1 M potassium phosphate buffer at pH 8, where the Co-Pi thickness was controlled by varying the amount of charge passed, *i.e.*, the deposition duration as described previously.[33] Masks of black electrical tape with 6 mm apertures were applied onto all working electrodes for defined active surface areas.

Physical measurements. Photoelectrochemical (PEC), electrochemical (EC), and electrochemical impedance spectroscopy (PEIS) measurements were conducted in a three-electrode configuration with the photoanode as the working electrode, Ag/AgCl as the reference electrode, and Pt as the counter electrode. A Gamry Series G 300 potentiostat with a frequency response analyzer was used for all measurements. All PEC measurements were performed in 0.1M KPi pH8 under backside illumination with calibrated 1 sun simulated AM 1.5 irradiation using an Oriel 96000 solar simulator equipped with a 150 W Xenon arc lamp and an Oriel AM 1.5 filter. Steady state photocurrent densities were taken as the current density after 100 seconds under illumination at a given applied potential. Impedance data were gathered using a 10 mV amplitude perturbation at frequencies between 20,000 and 0.01 Hz, with a 100 sec conditioning period prior to each potential measured to achieve a steady-state current density. Data were fit using Gamry Echem Analyst fitting software package. Potentials vs the reversible hydrogen electrode (RHE) were calculated using the Nernst equation, $V_{RHE} = V_{Ag/AgCl} + 0.0591(pH) + 0.1976$ V. All photocurrent-voltage and current-voltage data were collected at a scan rate of 10mV/s unless otherwise stated. Steady-state PEC current densities were collected after 60 sec.

Results and Analysis

Figure 1 plots three photocurrent-voltage (*J-V*) response curves measured for the same α-Fe_2O_3 photoanode after deposition of Co-Pi at three different thicknesses, each under the same backside-illumination conditions (see Experimental). Upon deposition of ~2.3 nm thick ("optimized"[33]) Co-Pi, the photocurrent onset potential shifts in the negative direction by ~200 mV relative to the bare α-Fe_2O_3. Increasing the Co-Pi thickness to ~24.6 nm ("bottlenecked"[31,33]) yields reduced PEC current densities at all potentials. The increased current density at ~1.8 V in the bottlenecked photoanode reflects the onset of dark current from Co-Pi-catalyzed water oxidation. From the bare α-Fe_2O_3, increasing the Co-Pi thickness thus initially shifts the onset potential in the negative direction before it reaches a minimum and again shifts in the positive direction (see Supporting Information). These data are consistent with our previous observations.[31,33]

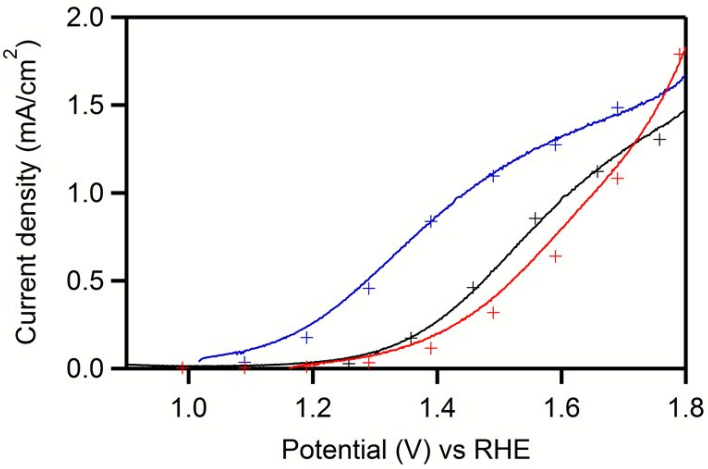

Figure 1. Photoelectrochemical current-voltage (*J-V*) curves measured for bare (black), optimized (~2.3 nm Co-Pi, blue), and bottlenecked (~24.6 nm Co-Pi, red) Co-Pi/α-Fe_2O_3 composite photoanodes in 0.1 M KPi buffer at pH 8. Measurements were performed using simulated AM 1.5 illumination of the photoanodes from the back side. The curves indicate data collected with a scan rate of 10mV/s. The + symbols indicate steady-state photocurrent densities after 100 seconds under illumination at the specified applied potential.

To probe the effects of Co-Pi thickness in more detail, photoelectrochemical impedance spectroscopy (PEIS) was performed on each of the three samples. Figure 2a shows Nyquist plots measured for the bare α-Fe_2O_3 and optimized Co-Pi/α-Fe_2O_3 photoanodes under backside illumination at +1.25 V. Two domains are clearly visible for each sample. For reference, the blue

data show a typical Nyquist plot for Co-Pi on FTO measured in the dark at +1.8 V vs RHE. Here, only a single semicircle is observed, similar to Co-Pi/α-Fe_2O_3 photoanodes under dark conditions.

Figure 2b shows the simplified equivalent circuit (SEC) frequently used to model α-Fe_2O_3 electrochemical impedance data under illumination.[18,39,42,43] This SEC consists of series resistance (R_s), resistance from trapping of photogenerated conduction-band electrons (R_{trap}), and charge-transfer resistance from either α-Fe_2O_3 surface states or Co-Pi to water ($R_{CT\ SS,\ Co\text{-}Pi}$). The SEC also includes two capacitor elements: the capacitance of the bulk space-charge region and Helmholtz layer (C_{bulk}), and the minority (hole) capacitance of the surface states associated with α-Fe_2O_3 (C_{SS}) or Co-Pi ($C_{Co\text{-}Pi}$).

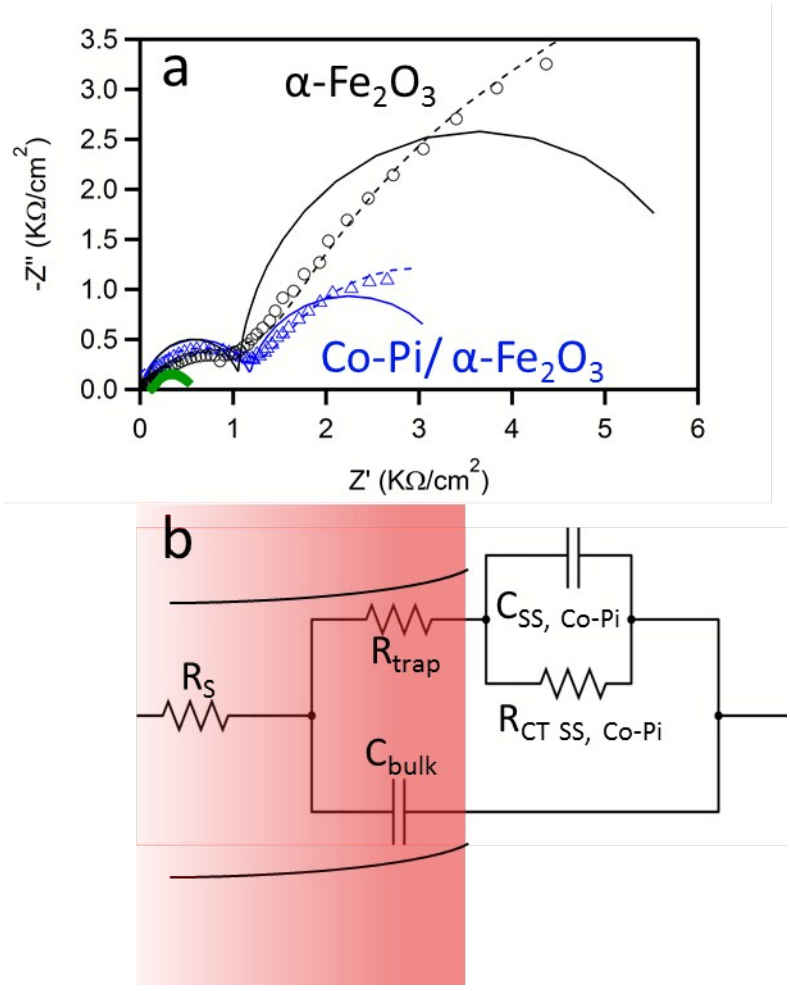

Figure 2. Nyquist plots for bare α-Fe_2O_3 (black, open circles) and optimized (~2.3 nm Co-Pi, blue open triangles) Co-Pi/α-Fe_2O_3 photoanodes measured at +1.25 V vs RHE, and for an FTO electrode with a ~490 nm-thick Co-Pi layer measured at +1.8 V vs RHE (green, open diamonds). The solid lines show fits to the data using a standard capacitor

element, and the dashed lines shows fits using a CPE. (b) The equivalent circuit used to model the impedance spectra when two domains are visible. A simple Randles circuit was used for the Co-Pi/FTO electrochemical impedance data, where only one domain is visible.

The asymmetries of the Nyquist plots (relative to semicircles) are due to frequency dispersion detected in the impedance measurement.[44,45] Such dispersion is typical for rough surfaces with large populations of surface states. In light of this dispersion, the data were analyzed in two ways: (a) using a constant phase element (CPE), and (b) using a standard capacitor. The CPE analysis is often preferred for asymmetrical EIS data.[44,45] We find that the CPE and capacitor analyses yield similar results here, lending credence to the conclusions drawn from these analyses. Although the capacitor model underestimates the resistance for the charge-transfer semicircle slightly, it yields unique fits at low potentials (<+1.4 V) where the CPE analysis generally does not. In addition, modeling EIS data with a CPE contains an extra fitting parameter that damps –Z" relative to Z' in the Nyquist plot but has no physical significance (see Supporting Information). For these reasons, the results presented here are those obtained using the standard capacitor analysis. For completeness, however, the analogous results obtained from the CPE analysis and statistical significance plots are provided as Supporting Information. For the Co-Pi/FTO sample, where only a single semicircle is visible in the Nyquist plot, a simple Randles circuit consisting of a series resistance (R_S) element followed by a parallel *RC* circuit (R_{CT}, C_{TOT}) was used.

Figure 3a plots $R_{CT\ SS}$, C_{SS}, and the *J-V* curve for the bare α-Fe_2O_3 photoanode measured under AM 1.5 backside illumination. Similar to planar α-Fe_2O_3 photoanodes,[17,18,42] C_{SS} maximizes and $R_{CT\ SS}$ drops at the onset potential for PEC water oxidation. The peak capacitance is ~1 mF/cm^2, which is consistent with values measured for planar films[18] after taking into account the surface roughness factor of ~20 in the present mesostructures.[41] On planar α-Fe_2O_3 photoanodes, PEIS measurements and spectroelectrochemical data have revealed that charge transfer from the semiconductor surface to the electrolyte proceeds through a series of surface-state-mediated steps involving high-oxidation-state iron species (Fe^{4+}, Fe^{5+}).[17,18,39,42] Surface states have also been observed on mesostructured α-Fe_2O_3.[15,20,21,37,46] From the similarities in C_{SS}, $R_{CT\ SS}$, and the PEC *J-V* curves between planar and mesostructured α-Fe_2O_3, we conclude that charge transfer at the mesostructured α-Fe_2O_3 surface proceeds through a similar pathway as

at the planar α-Fe_2O_3 surface.

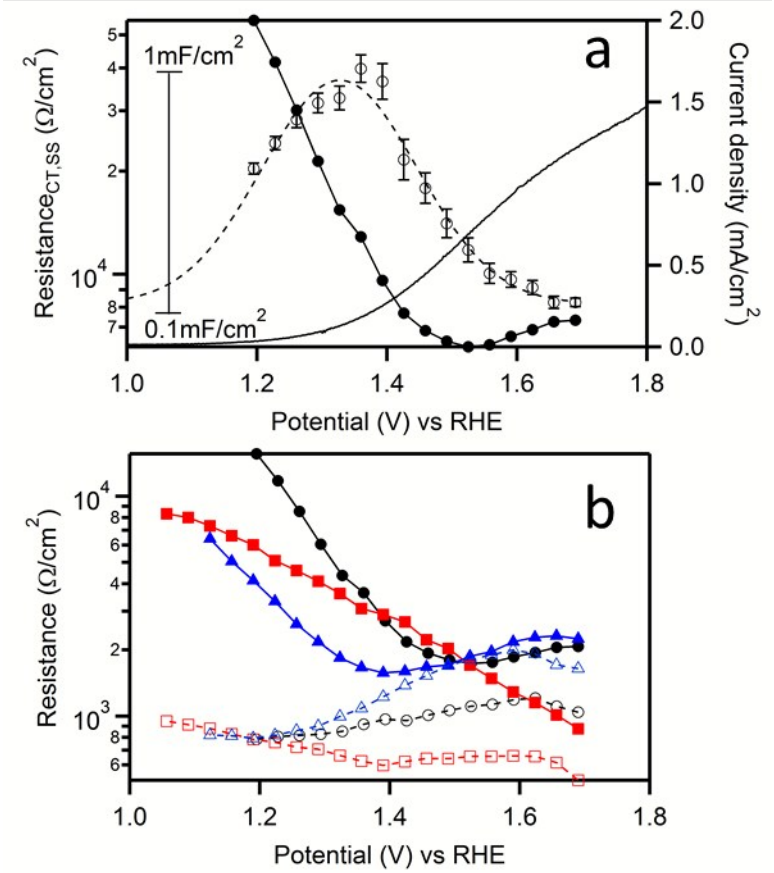

Figure 3. (a) Photoelectrochemical $R_{CT\ SS}$ (closed circles), C_{SS} (open circles), and *J-V* (solid line) data measured for a bare α-Fe_2O_3 photoanode, plotted vs applied potential. The inset scale bar refers to C_{SS}. The dashed line is a guide to the eye. The error bars represent uncertainties from the impedance fitting. **(b)** $R_{CT\ SS,\ Co\text{-}Pi}$ (solid symbols, solid lines) and R_{trap} (open symbols, dashed lines) of 0 (bare α-Fe_2O_3, black circles), ~2.3 (optimized Co-Pi/α-Fe_2O_3, blue triangles) and ~24.5 nm Co-Pi ("bottlenecked", red squares) on the same α-Fe_2O_3 photoanode, plotted vs applied potential.

Figure 3b plots $R_{CT\ SS,\ Co\text{-}Pi}$ and R_{trap} vs applied potential for the bare α-Fe_2O_3 photoanode as well as for the optimized and bottlenecked Co-Pi/α-Fe_2O_3 photoanodes. Apart from a -200 mV shift, $R_{CT\ Co\text{-}Pi}$ for the optimized composite photoanode closely resembles $R_{CT\ SS}$ for the bare α-Fe_2O_3 photoanode. In contrast, $R_{CT\ Co\text{-}Pi}$ for the bottlenecked photoanode exhibits behavior more characteristic of Co-Pi on FTO (see Supporting Information). A similar evolution from α-Fe_2O_3-like to Co-Pi-like kinetics with increasing Co-Pi thickness was also observed in the pH dependence of Co-Pi/α-Fe_2O_3 PEC measurements.[33]

For all Co-Pi thicknesses, R_{trap} behaves similarly at potentials more negative of ~+1.2 V,

but as the potential is swept more positive, a clear dependence on Co-Pi thickness emerges. R_{trap} of the optimized Co-Pi/α-Fe_2O_3 photoanode increases relative to the bare photoanode to a maximum of 2000 Ω/cm^2 at +1.6 V, and R_{trap} for the bottlenecked photoanode decreases. Because R_{trap} probes conduction-band-electron trapping, changes in this parameter with the addition of Co-Pi suggest that Co-Pi influences surface electron-hole recombination (*vide infra).* As a cross check, the total resistance calculated from the PEIS analysis ($R_{TOT} = R_s + R_{trap} + R_{CT\ SS,\ Co\text{-}Pi}$) was plotted vs applied potential and compared with the differential resistance (dV/dI) obtained directly from the *J-V* data, plotted in the same way. These two independent data sets agree well (see Supporting Information).

Figure 4 compares capacitance values measured for illuminated Co-Pi/α-Fe_2O_3 photoanodes with those of Co-Pi/FTO electrodes measured in the dark. Figure 4a plots $C_{Co\text{-}Pi}$ data overlaid with the *J-V* curves for optimized and bottlenecked Co-Pi thicknesses on the same α-Fe_2O_3 photoanode. As with the bare α-Fe_2O_3 photoanode, these data show maxima in $C_{Co\text{-}Pi}$ near the onset potentials for PEC water oxidation, where the maximum $C_{Co\text{-}Pi}$ scales with Co-Pi thickness. The increasing $C_{Co\text{-}Pi}$ with increasing Co-Pi thickness is interpreted as reflecting hole storage within Co-Pi. For example, if this increase in capacitance were the result of hole storage within α-Fe_2O_3 itself, then every Fe^{3+} within ~3 nm of the surface must be formally oxidized to Fe^{4+} to accommodate this charge accumulation (given a unit cell volume of ~34.8 nm^3, six Fe_2O_3 formula units per unit cell, and a surface-area-to-volume ratio of 20, ref. 41). Similar capacitance values have been measured on planar Co-Pi/α-Fe_2O_3 films in which the charge capacity is nearly equal to the total number of Fe^{3+} ions in the film.[39] Such transformations would require a far greater applied potential, or the hematite surface would have to be permeable to electrolyte ions for charge compensation. Neither of these scenarios is considered probable given the close proximity and redox properties of Co-Pi. The increasing capacitance with increasing Co-Pi thickness is thus attributed to hole storage within Co-Pi, confirming hole transfer from α-Fe_2O_3 to Co-Pi.

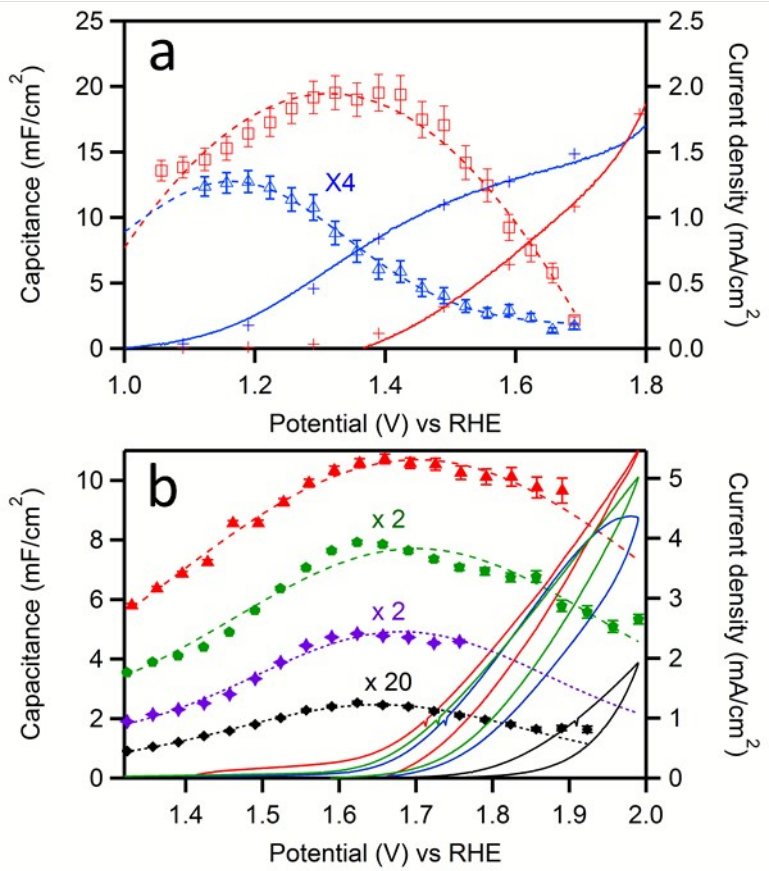

Figure 4. (a) $C_{SS\ Co\text{-}Pi}$ (open symbols) and *J-V* (hash marks) data measured for ~2.3 nm (blue triangles) and ~24.5 nm (red circles) Co-Pi thicknesses on the same α-Fe_2O_3 photoanode, plotted vs applied potential. Measurements used backside AM 1.5 illumination in 0.1 M KPi at pH 8. The symbols on the *J-V* curves represent steady-state current densities. **(b)** C_{TOT} (markers) and dark *J-V* (solid lines) data measured at 10 mV/s scan rate for ~1.2 (black closed diamonds), ~24.5 (purple closed stars), ~46.8 (green closed pentagons), and ~490 nm (red closed triangles) Co-Pi thicknesses on planar FTO, plotted vs applied potential. The dashed lines on the $C_{Co\text{-}Pi,\ TOT}$ data are guides to the eye.

The difference in potential between the two peak capacitances (~180 mV) is essentially the same as the difference in photocurrent onset potentials (~200 mV). Figure 4b shows the dark cyclic-voltammetry and EIS C_{TOT} data for four Co-Pi thicknesses on FTO. These *J-V* curves follow the trends reported previously for Co-Pi electrocatalysis.[27,28,30,47] For all Co-Pi thicknesses, electrocatalysis is preceded by a maximum in C_{TOT}. Importantly, C_{TOT} for the Co-Pi/FTO electrodes maximizes at nearly the same applied potential regardless of Co-Pi thickness. In contrast, the maximum in C_{TOT} shifts with Co-Pi thickness in the Co-Pi/α-Fe_2O_3 photoanodes

(Fig. 4a). The shift in $C_{SS\ Co\text{-}Pi}$ between optimized and bottlenecked Co-Pi/α-Fe_2O_3 photoanodes suggests that this PEC water oxidation is kinetically limited. Under thermodynamic control in the dark, the Fermi level of the electrocatalytic cell is dictated by the applied potential, and the peak capacitance therefore occurs at approximately the same potential regardless of Co-Pi thickness (Fig. 4b). Under AM 1.5 illumination in a thermodynamically limited regime, the driving force for catalytic turnover is determined by the potential of the holes entering the Co-Pi layer. In this case, the peak capacitance would also occur close to the same potential regardless of Co-Pi thickness. In a kinetically limited regime, however, the peak capacitance (and thus the current density) depends on the Co-Pi thickness. The positive shift in the peak $C_{Co\text{-}Pi}$ with increasing Co-Pi thickness observed in Fig. 4a thus implicates a Co-Pi-induced kinetic barrier in the bottlenecked Co-Pi/α-Fe_2O_3 photoanodes, *i.e.*, thick Co-Pi layers introduce kinetic limitations to the current densities achievable in mesostructured Co-Pi/α-Fe_2O_3 composite photoanodes.

Co-Pi shows first-order charge-transfer kinetics under electrochemical conditions, where a reversible proton-coupled electron transfer step is thought to precede the rate-determining O-O bond-formation step.[29,30] The rate-determining electron-transfer step for water-oxidation catalysis at the surface of α-Fe_2O_3 has also been described by a phenomenological charge-transfer rate constant (k_{CT}).[22,48] Likewise, recombination of photogenerated holes with conduction-band electrons can be parameterized phenomenologically by k_{rec}. Taking bulk recombination (>~5nm from the SCLJ) as independent of surface modification, PEC water oxidation is thus governed by the balance between k_{CT} and k_{rec}. k_{CT} can be obtained directly from PEIS data as the frequency at the maximum phase angle of the charge-transfer semicircle in the Nyquist plot (the RC time constant).

The resistance parameters measured by PEIS (R_{trap} and R_{CT}) and the rate constants k_{CT} and k_{rec} are related as described by equation 1,[16,49] where k_{trap} is the electron-trapping rate constant, n is the electron density (taken to be constant at constant illumination intensity), and $\gamma(V)$ is the probability of electron-trap occupation at a given trap energy and applied potential (V).

$$\frac{R_{trap}}{R_{CT}} = \frac{k_{CT}}{(nk_{trap}+k_{rec})} = \gamma(V)\frac{k_{CT}}{k_{rec}} \quad (1)$$

$\gamma(V)$ has the functional form described by equation 2, where E_{F_0} is the Fermi level at equilibrium, E_T is the energy of the electron trap, q is the elementary charge, and k_B is the Boltzmann constant.

$$\gamma(V) = \left[1 + e^{\frac{E_{F_0} - E_T}{k_B T}} * e^{\frac{-qV}{k_b T}}\right]^{-1} \quad (2)$$

Electron traps at α-Fe_2O_3 surfaces lie within a few hundred meV of the conduction-band edge (< 300 meV),[21,36] and consequently $\gamma(V)$ is essentially unity at the potentials of interest (>+1.2 V vs RHE, see Supporting Information for details), simplifying eq 1.

Figure 5 summarizes the PEIS results and analysis. From Fig. 5a, k_{CT} for the bare electrode is constant at ~1 s^{-1} at potentials below +1.3 V vs RHE. When the potential is swept more positive, k_{CT} increases to ~6.6 s^{-1} at +1.56 V vs RHE. At the ideal SCLJ, k_{CT} would be independent of voltage. This change in k_{CT} thus implicates a potential drop across the Helmholtz layer, likely because of Fermi-level pinning. By changing the electronic environment within the Helmholtz region, the transition-state energy is lowered and k_{CT} increases.[16] Fermi-level pinning in aqueous electrolyte has been observed with α-Fe_2O_3 photoelectrodes and is proposed to be a primary cause for the overpotentials required to drive PEC water oxidation.[16,18-21,39] For the optimized composite photoelectrode, a similar increase with potential is seen, but k_{CT} is smaller than in the bare electrode at all potentials. k_{CT} decreases even further when a thick Co-Pi layer is deposited. This decrease in k_{CT} with increasing Co-Pi thickness is surprising given that Co-Pi is a competent water-oxidation electrocatalyst[27,28,30] and that at low applied potentials (> +1.3 V) PEC OER catalysis proceeds primarily through Co-Pi in mesostructured Co-Pi/α-Fe_2O_3 composite photoanodes.[33]

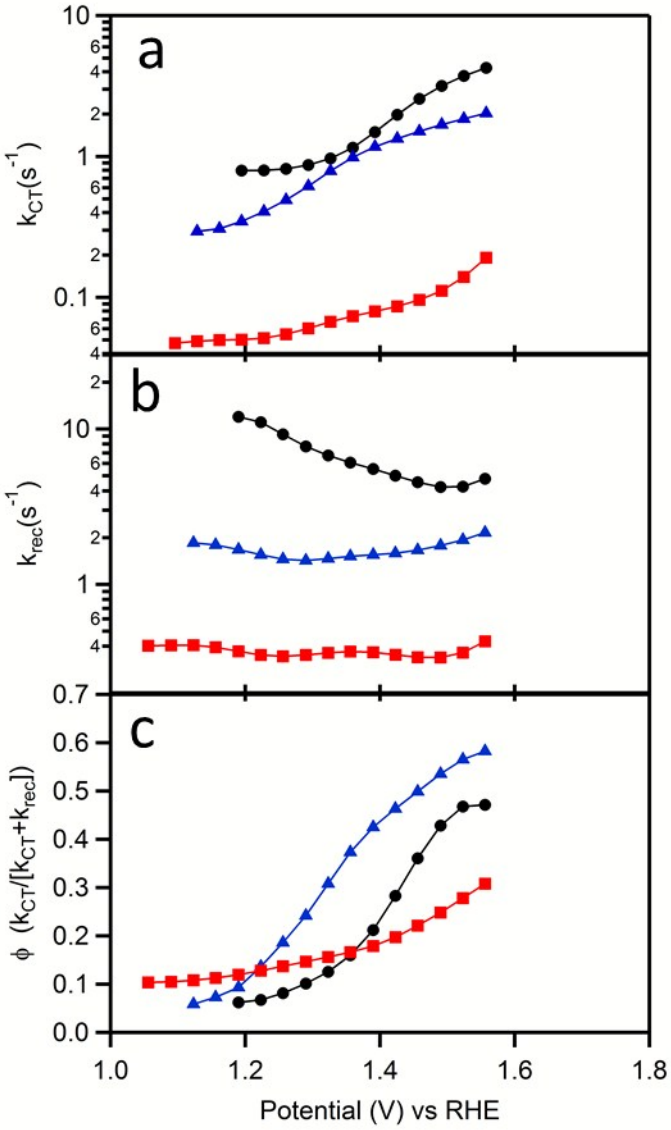

Figure 5. (a) Charge-transfer rate constants (k_{CT}), **(b)** recombination rate constants (k_{rec}), and **(c)** water-oxidation quantum efficiencies for bare α-Fe_2O_3 (black circles), 2.3 nm Co-Pi/α-Fe_2O_3 (blue triangles), and 24.5 nm Co-Pi/α-Fe_2O_3 (red squares) photoanodes determined from the analysis of PEIS data, all plotted vs applied potential.

The recombination rate constants (k_{rec}) for bare, optimized, and bottlenecked Co-Pi/α-Fe_2O_3 photoanodes deduced from the PEIS analysis are plotted in Fig. 5b. Consistent with previous reports,[15,16,18,37] k_{rec} of the bare α-Fe_2O_3 photoanode at +1.2 V vs RHE is one order of magnitude larger than k_{CT} at the same potential (11 vs 1 s^{-1}). This slow charge transfer relative to

recombination prevents Faradaic current flow, as reflected in the very small PEC currents observed at these potentials (Fig. 1). As expected, k_{rec} decreases with increasing positive bias, and at +1.56V it is approximately equal to k_{CT}. Meaningful values for k_{rec} at more positive potentials were not attainable. Interestingly, upon addition of Co-Pi at its optimized thickness, k_{rec} is reduced by a factor of ~2 to 5 throughout the entire potential window. The bottlenecked photoelectrode shows an even greater decrease in k_{rec}, by a factor of ~10 to 50 relative to α-Fe_2O_3. For both Co-Pi thicknesses, k_{rec} is largely independent of the applied bias. In the absence of Co-Pi, all recombination must occur either within the bulk or at the α-Fe_2O_3 surface, and k_{rec} is expected to decrease as potential is increased and the depletion region is expanded.[37] When k_{rec} is independent of applied bias, however, the limiting recombination involves charges that are electronically decoupled from the semiconductor (*e.g.*, stored within the Co-Pi). Electronic decoupling is expected of materials that form a so-called 'adaptive junction'.[24,50] Therefore, we assign k_{rec} to recombination at the Co-Pi/α-Fe_2O_3 interface that is limited by the flux of Co-Pi holes to the α-Fe_2O_3 surface.

The PEIS parameters detailed above now allow the water-oxidation quantum efficiency to be calculated as the charge-transfer branching ratio, as described by equation 3.

$$\varphi = \frac{k_{CT}}{k_{CT}+k_{rec}} \quad (3)$$

Figure 5c plots this quantum efficiency vs potential. These quantum-efficiency plots, deduced entirely from analysis of PEIS data, agree remarkably well with the *J-V* data for the same samples presented in Fig. 1. This agreement illustrates that the shapes of the PEC *J-V* curves with and without Co-Pi are determined by the competition between charge-transfer and recombination processes at the α-Fe_2O_3 surface. Analysis of the individual rate constants used to generate these curves thus provides valuable new insight into the microscopic effects of Co-Pi on α-Fe_2O_3 PEC water oxidation.

Consistent with previous reports,[15,16,18,37] this analysis shows that the bare α-Fe_2O_3 photoanode is limited by fast recombination (large k_{rec}) despite its relatively favorable charge-transfer kinetics. Little photocurrent occurs at potentials where band bending is insufficient to slow this recombination. In contrast, the bottlenecked Co-Pi/α-Fe_2O_3 photoanode is limited by slow charge transfer (small k_{CT}), in spite of a k_{rec} that has been substantially reduced relative to α-Fe_2O_3. The optimized Co-Pi/α-Fe_2O_3 photoanode balances this *decrease* in k_{CT} against the concomitant *decrease* in k_{rec} to yield a net *increase* in photocurrent density at low potentials. The

same conclusion is drawn when the EIS data are modeled using a constant phase element (CPE) instead of a capacitor (see Supporting Information).

Discussion

The primary function of the Co-Pi electrocatalyst when deposited on the surface of α-Fe_2O_3 can now be understood. α-Fe_2O_3 is a self-limiting photoanode in which positive surface charge accumulation inhibits band bending through quasi-Fermi-level pinning, leading to rapid electron-hole recombination at low applied bias (Fig. 6). We propose that the primary role of Co-Pi is to provide an alternative pathway for water oxidation that avoids positive charge accumulation at the α-Fe_2O_3 surface. With thin Co-Pi layers, photogenerated holes can either be transferred to Co-Pi or trapped at the α-Fe_2O_3 surface. Holes collected by Co-Pi reduce the surface hole concentration, relieving to a degree the pinned quasi-Fermi level, which in turn expands the depletion region and reduces surface electron-hole recombination at less positive potentials. Thicker Co-Pi layers almost completely eliminate the native surface-state charge-transfer water-oxidation pathway, allowing the semiconductor to behave in a more ideal fashion, where VB holes are only transferred to Co-Pi. The slower water oxidation by Co-Pi relative to α-Fe_2O_3 promotes interfacial recombination between photogenerated α-Fe_2O_3 conduction-band electrons and Co-Pi holes, however, leading to the "kinetic bottleneck" phenomenon observed in mesostructured Co-Pi/α-Fe_2O_3 photoanodes.[7,31,33]

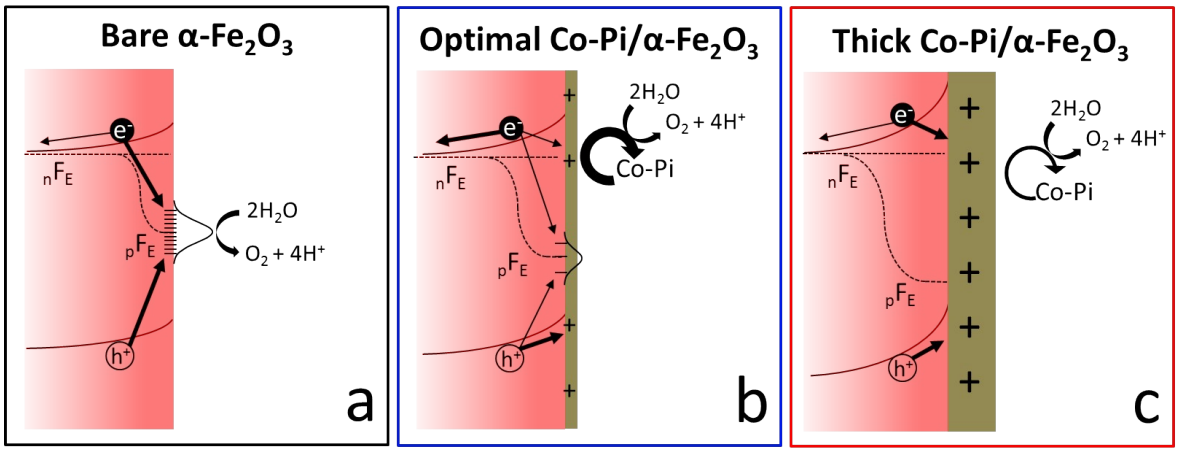

Figure 6. Schematic illustration of the recombination and charge-transfer pathways of α-Fe_2O_3 photoanodes with **(a)** no, **(b)** a thin (optimized), and **(c)** a thick (bottleneck) Co-Pi layer on their surfaces, each under illumination at potentials negative of +1.5 V vs RHE. For bare α-Fe_2O_3, charge transfer proceeds through a surface-state-mediated pathway that

pins the hole quasi-Fermi level ($_pF_E$), resulting in fast recombination and little Faradaic current. For the same α-Fe_2O_3 photoanode with an optimized Co-Pi layer, an alternative water-oxidation pathway exists that decreases the surface charge, partially unpins the hole quasi-Fermi level, and promotes charge transfer from both α-Fe_2O_3 and Co-Pi to water. For the same α-Fe_2O_3 photoanode with a thick Co-Pi layer, the direct α-Fe_2O_3 surface-mediated charge-transfer pathway is eliminated, completely unpinning the hole quasi-Fermi level, and all water oxidation proceeds through Co-Pi. From (b) to (c), the increased capacitive accumulation of Co-Pi oxidizing equivalents (Co^{4+}) leads to increased interfacial recombination with photogenerated α-Fe_2O_3 conduction-band electrons, limiting Faradaic current flow in (c) relative to (b).

Although it is not clear exactly why k_{CT} decreases with increasing Co-Pi thickness, one hypothesis is that this decrease stems from a decrease in the Co-Pi hole density as the Co-Pi thickness (volume) is increased, which reduces the turnover frequency per cobalt and elongates the hole residence time. These changes create greater opportunity for interfacial recombination. Another possibility is that Co^{4+} intermediates are stabilized in thick Co-Pi layers, increasing the barrier to O-O bond formation and hence again elongating the hole residence time. Long lived Co^{4+} intermediates in thick Co-Pi films have been observed by EPR and X-ray spectroscopies.[29,51] In any case, it appears that Co-Pi thickness tunes the balance between surface recombination and charge-transfer kinetics, and in mesostructured α-Fe_2O_3 photoanodes the optimal balance occurs at small Co-Pi thicknesses. At this optimal thickness, water oxidation is catalyzed by Co-Pi at the onset potential and is catalyzed directly at the α-Fe_2O_3 surface at greater applied potentials.[33] The picture that emerges from these studies thus contains elements from both leading hypotheses about the mechanism by which Co-Pi enhances the PEC performance of α-Fe_2O_3 photoanodes, and helps to reconcile the results from transient absorption and photoelectrochemical measurements within a unified interpretation.

Conclusion

The primary function of Co-Pi when interfaced with α-Fe_2O_3 photoanodes is to provide a water-oxidation pathway that does not involve α-Fe_2O_3 surface hole traps. Bypassing these traps unpins the hole quasi-Fermi level and allows the semiconductor to behave more ideally at less positive potentials. At optimal Co-Pi thicknesses, water oxidation is competitive against surface-state-mediated electron-hole recombination and oxygen evolution catalysis occurs. With thick Co-Pi layers, recombination between α-Fe_2O_3 electrons and Co-Pi holes attenuates photocurrents

at low potentials because of slow Co-Pi reaction kinetics. Although the results presented here were obtained using mesostructured α-Fe_2O_3 photoanodes prepared by APCVD, these insights should apply to other catalyst-modified photoanodes investigated for solar-driven photoelectrochemical water oxidation.

Acknowledgements

This work was supported by the US National Science Foundation (CHE-1213283) and partially conducted at the UW Nanotechnology User Facility, a member of the NINN.

References

(1) Fujishima, A.; Honda, K.: Electrochemical Photolysis of Water at a Semiconductor Electrode. *Nature* **1972**, *238*, 37-38.

(2) Lewis, N. S.; Nocera, D. G.: Powering the planet: Chemical challenges in solar energy utilization. *PNAS* **2006**, *103*, 15729-15735.

(3) Nocera, D. G.: Personalized Energy: The Home as a Solar Power Station and Solar Gas Station. *ChemSusChem* **2009**, *2*, 387-390.

(4) Bard, A. J.; Fox, M. A.: Artificial Photosynthesis: Solar Splitting of Water to Hydrogen and Oxygen. *Acc. Chem. Res.* **1995**, *28*, 141-145.

(5) Moomow, W.; Yamba, F.; Kamimoto, M.; Maurice, L.; Nyboer, J.; Urama, K.; Weir, T.: Introduction. In *IPCC Special Report on Renewable Energy Sources and Climate change Mitigation*; Edenhofer, O., Pichs-Madruga, R., Sokona, Y., Seyboth, K., Matschoss, P., Kadner, S., Zwickel, T., Eickemeier, P., Hansen, G., Schlömer, S., von Stechow, C., Eds.; Cambridge University Press: United Kingdom and New York, NY, USA, 2011.

(6) Khaselev, O.; Turner, J. A.: A Monolithic Photovoltaic-Photoelectrochemical Device for Hydrogen Production via Water Splitting. *Science* **1998**, *280*, 425-427.

(7) Zhong, D. K.; Cornuz, M.; Sivula, K.; Gratzel, M.; Gamelin, D. R.: Photo-assisted electrodeposition of cobalt-phosphate (Co-Pi) catalyst on hematite photoanodes for solar water oxidation. *Energy Environ. Sci.* **2011**, *4*, 1759-1764.

(8) Grätzel, M.: Photoelectrochemical cells. *Nature* **2001**, *414*, 338-344.

(9) Duret, A.; Grätzel, M.: Visible Light-Induced Water Oxidation on Mesoscopic α-Fe_2O_3 Films Made by Ultrasonic Spray Pyrolysis. *J. Phys. Chem. B* **2005**, *109*, 17184-17191.

(10) Osterloh, F. E.: Inorganic Materials as Catalysts for Photochemical Splitting of Water. *Chem. Mater.* **2007**, *20*, 35-54.

(11) Osterloh, F. E.: Inorganic nanostructures for photoelectrochemical and photocatalytic water splitting. *Chem. Soc. Rev.* **2013**, *42*, 2294-2320.

(12) Gardner, R. F. G.; Sweett, F.; Tanner, D. W.: The electrical properties of alpha ferric oxide—I.: The impure oxide. *J. Phys. Chem. Solids* **1963**, *24*, 1175-1181.

(13) Kennedy, J. H.; Frese, K. W.: Photooxidation of Water at α-Fe_2O_3 Electrodes. *J. Electrochem. Soc.* **1978**, *125*, 709-714.

(14) Dare-Edwards, M. P.; Goodenough, J. B.; Hamnett, A.; Trevellick, P. R.: Electrochemistry and photoelectrochemistry of iron(III) oxide. *J. Chem. Soc. Faraday Trans.* **1983**, *79*, 2027-2041.

(15) Le Formal, F.; Sivula, K.; Grätzel, M.: The Transient Photocurrent and Photovoltage Behavior of a Hematite Photoanode under Working Conditions and the Influence of Surface Treatments. *J. Phys. Chem. C* **2012**, *116*, 26707-26720.

(16) Upul Wijayantha, K. G.; Saremi-Yarahmadi, S.; Peter, L. M.: Kinetics of oxygen evolution at α-Fe_2O_3 photoanodes: a study by photoelectrochemical impedance spectroscopy. *Phys. Chem. Chem. Phys.* **2011**, *13*, 5264-5270.

(17) Hamann, T. W.: Splitting water with rust: hematite photoelectrochemistry. *Dalton Trans.* **2012**, *41*, 7830-7834.

(18) Klahr, B.; Gimenez, S.; Fabregat-Santiago, F.; Bisquert, J.; Hamann, T. W.: Electrochemical and photoelectrochemical investigation of water oxidation with hematite electrodes. *Energy Environ. Sci.* **2012**, *5*, 7626-7636.

(19) Klahr, B. M.; Hamann, T. W.: Current and Voltage Limiting Processes in Thin Film Hematite Electrodes. *J. Phys. Chem. C* **2011**, *115*, 8393-8399.

(20) Barroso, M.; Mesa, C. A.; Pendlebury, S. R.; Cowan, A. J.; Hisatomi, T.; Sivula, K.; Grätzel, M.; Klug, D. R.; Durrant, J. R.: Dynamics of photogenerated holes in surface modified α-Fe_2O_3 photoanodes for solar water splitting. *PNAS* **2012**, *109*, 15640-15645.

(21) Barroso, M.; Pendlebury, S. R.; Cowan, A. J.; Durrant, J. R.: Charge carrier trapping, recombination and transfer in hematite (α-Fe_2O_3) water splitting photoanodes. *Chem. Sci.* **2013**, *4*, 2724-2734.

(22) Pendlebury, S. R.; Cowan, A. J.; Barroso, M.; Sivula, K.; Ye, J.; Gratzel, M.; Klug, D. R.; Tang, J.; Durrant, J. R.: Correlating long-lived photogenerated hole populations with photocurrent densities in hematite water oxidation photoanodes. *Energy Environ. Sci.* **2012**, *5*, 6304-6312.

(23) Iandolo, B.; Wickman, B.; Zoric, I.; Hellman, A.: The rise of hematite: origin and strategies to reduce the high onset potential for the oxygen evolution reaction. *J. Mat. Chem. A* **2015**, *3*, 16896-16912.

(24) Lin, F.; Boettcher, S. W.: Adaptive semiconductor/electrocatalyst junctions in water-splitting photoanodes. *Nat. Mater.* **2014**, *13*, 81-86.

(25) Nocera, D. G.: The Artificial Leaf. *Acc. Chem. Res.* **2012**, *45*, 767-776.

(26) Moniz, S. J. A.; Shevlin, S. A.; Martin, D. J.; Guo, Z.-X.; Tang, J.: Visible-light driven heterojunction photocatalysts for water splitting - a critical review. *Energy Environ. Sci.* **2015**, *8*, 731-759.

(27) Kanan, M. W.; Nocera, D. G.: In Situ Formation of an Oxygen-Evolving Catalyst in Neutral Water Containing Phosphate and Co^{2+}. *Science* **2008**, *321*, 1072-1075.

(28) Kanan, M. W.; Surendranath, Y.; Nocera, D. G.: Cobalt-phosphate oxygen-evolving compound. *Chem. Soc. Rev.* **2009**, *38*, 109-114.

(29) Kanan, M. W.; Yano, J.; Surendranath, Y.; Dincă, M.; Yachandra, V. K.; Nocera, D. G.: Structure and Valency of a Cobalt−Phosphate Water Oxidation Catalyst Determined by in Situ X-ray Spectroscopy. *J. Am. Chem. Soc.* **2010**, *132*, 13692-13701.

(30) Surendranath, Y.; Kanan, M. W.; Nocera, D. G.: Mechanistic Studies of the Oxygen Evolution Reaction by a Cobalt-Phosphate Catalyst at Neutral pH. *J. Am. Chem. Soc.* **2010**, *132*, 16501-16509.

(31) Zhong, D. K.; Gamelin, D. R.: Photoelectrochemical Water Oxidation by Cobalt Catalyst ("Co−Pi")/α-Fe_2O_3 Composite Photoanodes: Oxygen Evolution and Resolution of a Kinetic Bottleneck. *J. Am. Chem. Soc.* **2010**, *132*, 4202-4207.

(32) Zhong, D. K.; Sun, J.; Inumaru, H.; Gamelin, D. R.: Solar Water Oxidation by Composite Catalyst/α-Fe_2O_3 Photoanodes. *J. Am. Chem. Soc.* **2009**, *131*, 6086-6087.

(33) Carroll, G. M.; Zhong, D. K.; Gamelin, D. R.: Mechanistic insights into solar water oxidation by cobalt-phosphate-modified α-Fe_2O_3photoanodes. *Energy Environ. Sci.* **2015**, *8*, 577-584.

(34) Barroso, M.; Cowan, A. J.; Pendlebury, S. R.; Grätzel, M.; Klug, D. R.; Durrant, J. R.: The Role of Cobalt Phosphate in Enhancing the Photocatalytic Activity of α-Fe_2O_3 toward Water Oxidation. *J. Am. Chem. Soc.* **2011**, *133*, 14868-14871.

(35) Gamelin, D. R.: Water splitting: Catalyst or spectator? *Nat. Chem.* **2012**, *4*, 965-967.

(36) Cowan, A. J.; Durrant, J. R.: Long-lived charge separated states in nanostructured semiconductor photoelectrodes for the production of solar fuels. *Chem. Soc. Rev.* **2013**, *42*, 2281-2293.

(37) Cummings, C. Y.; Marken, F.; Peter, L. M.; Tahir, A. A.; Wijayantha, K. G. U.: Kinetics and mechanism of light-driven oxygen evolution at thin film α-Fe_2O_3 electrodes. *Chem. Comm.* **2012**, *48*, 2027-2029.

(38) Liu, R.; Zheng, Z.; Spurgeon, J.; Yang, X.: Enhanced photoelectrochemical water-splitting performance of semiconductors by surface passivation layers. *Energy Environ. Sci.* **2014**, *7*, 2504-2517.

(39) Klahr, B.; Giménez, S.; Fabregat-Santiago, F.; Bisquert, J.; Hamann, T. W.: Photoelectrochemical and Impedance Spectroscopic Investigation of Water Oxidation with "Co-Pi" coated Hematite Electrodes. *J. Am. Chem. Soc.* **2012**, *134*, 16693-16700.

(40) Hamann, T. W.: Water splitting: An adaptive junction. *Nat. Mater.* **2014**, *13*, 3-4.

(41) Kay, A.; Cesar, I.; Grätzel, M.: New Benchmark for Water Photooxidation by Nanostructured α-Fe_2O_3 Films. *J. Am. Chem. Soc.* **2006**, *128*, 15714-15721.

(42) Klahr, B.; Hamann, T.: Water Oxidation on Hematite Photoelectrodes: Insight into the Nature of Surface States through In Situ Spectroelectrochemistry. *J. Phys. Chem. C* **2014**, *118*, 10393-10399.

(43) Le Formal, F.; Pendlebury, S. R.; Cornuz, M.; Tilley, S. D.; Grätzel, M.; Durrant, J. R.: Back Electron–Hole Recombination in Hematite Photoanodes for Water Splitting. *J. Am. Chem. Soc.* **2014**, *136*, 2564-2574.

(44) Salvarezza, R. C.; Arvia, A. J.: A Modern Approach to Surface Roughness Applied to Electrochemical Systems. In *Modern Aspects of Electrochemistry*; Conway, B. E., Bockris, J. O. M., White, R., Eds.; Springer US, 1996; Vol. 28; pp 289-373.

(45) Lasia, A.: Electrochemical Impedance Spectroscopy and its Applications. In *Modern Aspects of Electrochemistry*; Conway, B. E., Bockris, J. O. M., White, R., Eds.; Springer US, 2002; Vol. 32; pp 143-248.

(46) Sivula, K.: Metal Oxide Photoelectrodes for Solar Fuel Production, Surface Traps, and Catalysis. *J. Phys. Chem. Lett.* **2013**, *4*, 1624-1633.

(47) Surendranath, Y.; Dincă, M.; Nocera, D. G.: Electrolyte-Dependent Electrosynthesis and Activity of Cobalt-Based Water Oxidation Catalysts. *J. Am. Chem. Soc.* **2009**, *131*, 2615-2620.

(48) Cowan, A. J.; Barnett, C. J.; Pendlebury, S. R.; Barroso, M.; Sivula, K.; Grätzel, M.; Durrant, J. R.; Klug, D. R.: Activation Energies for the Rate-Limiting Step in Water Photooxidation by Nanostructured α-Fe_2O_3 and TiO_2. *J. Am. Chem. Soc.* **2011**, *133*, 10134-10140.

(49) Bertoluzzi, L.; Bisquert, J.: Equivalent Circuit of Electrons and Holes in Thin Semiconductor Films for Photoelectrochemical Water Splitting Applications. *J. Phys. Chem. Lett.* **2012**, *3*, 2517-2522.

(50) Mills, T. J.; Lin, F.; Boettcher, S. W.: Theory and Simulations of Electrocatalyst-Coated Semiconductor Electrodes for Solar Water Splitting. *Phys. Rev. Lett.* **2014**, *112*, 148304.

(51) McAlpin, J. G.; Surendranath, Y.; Dincă, M.; Stich, T. A.; Stoian, S. A.; Casey, W. H.; Nocera, D. G.; Britt, R. D.: EPR Evidence for Co(IV) Species Produced During Water Oxidation at Neutral pH. *J. Am. Chem. Soc.* **2010**, *132*, 6882-6883.

TOC Graphic